



Jet-entrainment sampling: A new method for extracting particles from flames

Hope A. Michelsen^{a,b,*}, Emeric Boigné^{c,*}, Paul E. Schrader^b,
 K. Olof Johansson^{b,d}, Matthew F. Campbell^{b,e}, Ray P. Bambha^b,
 Matthias Ihme^c

^a Department of Mechanical Engineering, University of Colorado Boulder, Boulder, CO 80309 USA

^b Combustion Research Facility, Sandia National Laboratories, Livermore, CA, 94550, USA

^c Department of Mechanical Engineering, Stanford University, Stanford, CA, 94305, USA

^d Now at KLA Corporation, Milpitas, CA, 95035, USA

^e Now at Department of Mechanical Engineering and Applied Mechanics, University of Pennsylvania, Philadelphia, PA, 19104, USA

Received 5 January 2022; accepted 15 July 2022

Available online xxx

Abstract

We have developed a new method for extracting particulates and gas-phase species from flames. This technique involves directing a small jet of inert gas through the flame to entrain the sample, which is then collected by a probe on the other side of the flame. This sampling technique does not require inserting a probe or sampling surface into the flame and thus avoids effects on the flame due to conductive cooling by the probe and recombination, quenching, and deposition reactions at the sampling surface in contact with the flame. This approach thus allows for quenching and diluting the sample during extraction while minimizing the perturbations to the flame that have a substantial impact on flame chemistry. It also circumvents clogging of the probe with soot, a problem that commonly occurs when a probe is inserted into a hydrocarbon-rich premixed or diffusion flame. In this paper, we present experimental results demonstrating the application of this technique to the extraction of soot particles from a co-flow ethylene/air diffusion flame. The extracted samples were analyzed using transmission electron microscopy (TEM), and the results are compared with measurements using *in situ* diagnostics, *i.e.*, laser-induced incandescence and small-angle X-ray scattering. We also compare TEM images of particles sampled using this approach with those sampled using rapid-insertion thermophoretic sampling, a common technique for extracting particles from flames. In addition, we have performed detailed numerical simulations of the flow field associated with this new sampling approach to assess the impact it has on the flame structure and sample following extraction. The results presented in this paper demonstrate that this jet-entrainment sampling technique has significant advantages over other common sample-extraction methods.

© 2022 The Combustion Institute. Published by Elsevier Inc. All rights reserved.

Keywords: Soot; Sampling; Flame; TEM; Particles

* Corresponding authors.

E-mail address: Hope.Michelsen@colorado.edu (H.A. Michelsen).

<https://doi.org/10.1016/j.proci.2022.07.140>

1540-7489 © 2022 The Combustion Institute. Published by Elsevier Inc. All rights reserved.

1. Introduction

Soot is well known for both wide-ranging commercial uses and detrimental effects on human health, air quality, and climate. Nevertheless, there is a poor understanding of the physical and chemical mechanisms that control its formation and evolution.

The production of soot and other particles in flames is highly sensitive to flame conditions [1,2]. Developing an understanding of the chemical and physical mechanisms that control particle production and properties requires diagnostics that deliver information about particle size, morphology, abundance, and composition. *In situ* diagnostics are desirable but challenging [3,4], typically involving laser or X-ray probes with extensive, complex analyses. *Ex situ* diagnostics on particles sampled from flames can provide information about particle characteristics. The sampling probes used for *ex situ* analysis are flame-intrusive, however, and perturb local flame conditions, such as temperature, flow field, and chemical composition, e.g., [5–23]. For *ex situ* sampling, it is critical to minimize impacts of the sampling probe on the combustion conditions, which can influence the particle characteristics prior to extraction. It is also important to minimize impacts of sampling processes on the particles after extraction.

There are several approaches that are commonly used to sample particles from flames. One approach for offline measurements, such as transmission electron microscopy (TEM) imaging and laser microprobe mass spectrometry (LMMS), involves thermophoretic sampling by rapid insertion and retraction of a cool substrate into and out of the flame using a pneumatic device, e.g., [11,13,22–31]. Another approach involves installation of a metal tube across the flame with an inlet pinhole often positioned at the flame axial centerline, e.g., [19,32–34]. Inert gas is flowed through the metal probe, and particles are drawn into the probe through the hole and rapidly cooled and diluted by the inert gas. This approach is used for online measurements, such as scanning mobility particle sizing (SMPS), aerosol particle mass analysis (APM), and aerosol mass spectrometry (AMS). A modification of this approach embeds the dilution tube with the inlet orifice inside a metal stabilization plate for online *ex situ* measurements, e.g., [2,17,35]. Alternatively, a quartz or metal tube is inserted into the flame from the side or top of the flame, and particles are drawn from the flame using an ejector pump or other vacuum system, e.g., [32,34,36–39]. Attempts have been made to introduce dilution at the inlet tip of this type of probe with a coaxial counter-flow of inert gas that mixes with the sampled gas at the probe tip in the flame [33,40].

Previous studies have shown that the use of any of these probes significantly lowers flame tempera-

tures near the probe [14,17,19,35]. Use of extractive sampling probes also leads to radical destruction and other perturbations to the chemical composition in the vicinity of the probe [5–10, 12,15,16,18]. These effects, in addition to effects on the flow field, can enhance particle nucleation and aggregation in the flame [11,14]. In addition, probe sampling can significantly influence particle size distributions through (1) size-dependent collection efficiencies [13] and (2) coagulation and adsorption of gas-phase species in the sampling probe, especially when sampling from regions of the flame where new particles are formed [34]. There is thus a need for new *in situ* diagnostics and probe-sampling techniques.

In this paper, we assess the utility of jet-entrainment sampling (JES), a new method for sampling from a flame that avoids insertion of a probe into the flame and associated perturbations on flame and sample conditions. This new approach involves forcing a small jet of inert gas through the flame. This jet of gas entrains and dilutes flame gases and particles, which are then captured in a collection tube on the opposite side of the flame. We have performed simulations of the temperature and flow field to assess the impact of this extraction method on the entrained samples prior to and during extraction. Section 2 summarizes the measurement method, experimental setup, and simulation approach. Section 3 presents comparisons with *in situ* measurements and a computational flow-field analysis, quantifying the effect of the jet entrainment on the sampling. Conclusions are presented in Section 4.

2. Measurement and simulation approaches

2.1. Burner and flame

The flame used in this study was a linear co-flow ethylene/air laminar diffusion flame produced by a linear Hencken burner, described previously [41]. The burner consists of 25 fuel tubes, each with an inner diameter of 508 μm , arranged in a line and embedded in a honeycomb mesh that supplies the co-flow of air. Flow rates of ethylene and air were chosen to generate Flame E1, as described by Campbell *et al.* [41]. The flow of ethylene was 0.200 standard liter per minute (SLM), relative to standard conditions of 0 $^{\circ}\text{C}$ and 1 atm, and the flow of air was 14.0 SLM. Flame E1 is ~ 3 mm wide and ~ 38 mm long. Flow rates were controlled using mass flow controllers (MKS Instruments, Inc. Model GM50A), calibrated (Sierra Instruments, Inc. Model SL-500) prior to use. The burner was mounted on a translation stage that allowed it to be moved vertically, and the burner body was maintained at a constant temperature of 20 $^{\circ}\text{C}$.

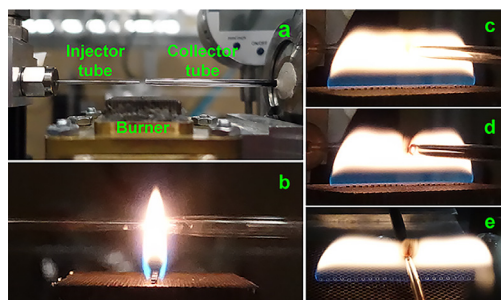


Fig. 1. Experimental setup for jet-entrainment sampling. Photos are shown of the setup viewing the burner (a) end on (*i.e.*, along the row of fuel tubes), (b) end on with the flame and sampling on, (c) from the side of the flame on the extractor side with sampling off, (d) from the same view as in (c) with sampling on, and (e) from the side of the flame on the injector side with sampling on.

2.2. Extractive sampling by jet entrainment

Fig. 1 shows the experimental setup for the jet-entrainment sampling (JES) method for extracting soot samples applied to Flame E1. Two quartz tubes with tapered tips are placed on opposite sides of the flame, perpendicular to the flame-gas flow and the line of fuel tubes, facing the flame and collinearly aligned with (or slightly offset vertically from) each other (Figs. 1a and 1b). This technique has been used previously [42] but has not been described or assessed in detail.

The injector tube (1-mm ID, 2-mm OD, tapered to 1.2-mm OD at the tip) supplies an inert gas horizontally through the flame, cutting the flame at the lower edge of the jet and trapping and entraining flame gas and soot particles. Here, N_2 was used with a flow rate of 0.5 SLM, which can be modified for different flame conditions and *ex situ* diagnostics. The injector tube is mounted *via* a stainless-steel Swagelok fitting with a Teflon ferrule on an *X-Y-Z* translation stage that allows the tube to be moved relative to the burner and the collector tube.

The entrained and diluted sample is then collected by the second quartz (collector) tube. In these experiments, the collector tube had a 3-mm OD and 2-mm ID and was tapered to a 2.2-mm OD at its tip. This tube is held in a stainless-steel fitting with a Teflon ferrule mounted in a temperature-stabilized copper block heated to $\sim 60^\circ\text{C}$ to reduce water condensation in the sampling line. A vacuum pump is used on the collector side to maintain the flow of gases into the collector. The vacuum is adjusted to prevent the flame from being sucked into the collector with the jet off. The pressure in the collector tube is actively stabilized relative to ambient pressure to maintain constant sample flow rate. Fig. 1c shows a photo of the flame from the collector side with the jet off, and Figs. 1d and 1e show the flame with the jet turned on to extract samples

from the flame. The tubes are separated from one another by 2.5 to 7.0 mm, depending on the flame and flame conditions. For TEM imaging, the collector tube was connected to a stainless-steel tee containing TEM grids mounted vertically, parallel to the sample flow, and particles were collected thermophoretically.

2.3. Thermophoretic extractive sampling

For comparison, we also extracted soot samples from Flame E1 using a rapid-insertion thermophoretic sampling (RITS) technique [41]. We used a double-actuating pneumatic piston cylinder with a 24-mm stroke (Parker Hannifin Corp. Model B511BB549C) to move the grids into and out of the flame perpendicular to the direction of flame-gas flow and the line of fuel tubes. Samples were collected on 3.05-mm-diameter copper mesh grids (Ted Pella #01,824 and #01,830), which were mounted on the pneumatic sampler parallel to the flame-gas flow. In-flame exposure times ranged from 40 to 100 ms, depending on height above burner (HAB). Samples were collected with the center of the grids at selected HABs and were imaged using TEM.

2.4. TEM imaging

TEM images were recorded using an electron microscope (JEOL USA, Inc. Model JEM-1200EX), fitted with an eleven-megapixel digital camera (Gatan, Inc. model ES1000W). Most images were recorded at 250,000-times magnification.

2.5. Flow-field simulations

We solved the multi-species reacting Navier-Stokes equations with detailed chemistry and buoyancy using LaminarSMOKE [43,44]. This compressible code is based on the OpenFOAM framework and integrates the stiff chemistry solver using the Strang operator splitting scheme. We used a detailed C1–C16 chemical mechanism with 452 species and 24,041 reactions for the unperturbed flame and a smaller C1–C3 mechanism with 114 species and 1991 reactions for the JES configuration, both from the CRECK modeling group [45,46].

Our simulations considered a symmetric domain that included 4.5 fuel tubes in the region $y > 0$ (y is the direction parallel to the line of fuel tubes), such that 9 of the 25 fuel injectors of the burner were modeled by applying symmetric boundary conditions at the $y = 0$ plane. The mesh consisted of a total of 1 million hexahedral elements at the finest cell resolution of $25\ \mu\text{m}$ at the fuel tubes, $50\ \mu\text{m}$ in the soot-formation region, and coarser in the far field. The fuel-tube exit was 0.25 mm above the honeycomb top plane. For the

low gas-flow rates investigated, the flame was non-adiabatic and stabilized close to the burner surface. The burner body was maintained at a temperature of 20 °C [41]. To capture this effect, we modeled the honeycomb in the CFD geometry using isothermal boundary conditions at 300 K. The walls of the fuel and quartz tubes, and the inlet flow of air, N₂, and fuel were also set to 300 K. Parabolic inflow profiles for velocity were prescribed for the fuel tubes and the JES injector tube. In the simulation of the JES soot probes, the two quartz tubes were placed at an HAB of 6 mm and separated by 14 mm. The tapered quartz tubes were simulated with a thickness of 0.1 mm at the tip, linearly growing to a thickness of 0.5 mm over a length of 5 mm from the tip. For the JES configuration, symmetric boundary conditions were imposed at the centerplane.

3. Results and discussion

3.1. TEM images of extracted particles

Fig. 2 shows a comparison of TEM images of particles extracted from Flame E1 using RITS and JES techniques. Results using the two techniques are qualitatively very different from one another at most HABs. RITS does not capture particles at an HAB of 3 mm. The particles captured by RITS at 4 mm (Fig. 2a) are spherical and ~20 nm in diameter. At HABs of 5 mm (Fig. 2b) and 6 mm (Fig. 2c), RITS captures particles that are spherical and nearly translucent to the electron beam. These images are very similar to those captured previously using RITS [24,25,27–29]. Such results have been instrumental in shaping our description of incipient and young soot particles as spherical and liquid-like [2,3,29,47]. At 7 mm (Fig. 2d), these particles abruptly transition to aggregates of monodisperse primary particles with significant necking or bridging between primary particles. This transition from sparse translucent singlets to large opaque aggregates has been observed many times using RITS in laminar diffusion flames, e.g., [26,27,29,48]. Extensive necking or bridging between primary particles in aggregates has also been observed in particles extracted from flames using RITS [31]. At 8 mm (Fig. 2e) and 9 mm (Fig. 2f), the extracted particles are aggregates of more clearly differentiated monodisperse primary particles, which is typical of mature soot particles [2,3,47]. At 8 and 9 mm, the aggregates are similar in size and morphology and are composed of similarly sized primary particles.

In contrast to RITS, JES captures particles at 3 mm; these particles are non-spherical blobby aggregates larger than ~50 nm (Fig. 2g). The primary particles within these coagulated structures have an average diameter of 27.0 ± 12.7 nm. JES captures similarly shaped particles at 4 mm (Fig. 2h), but, although the aggregates are approximately an order

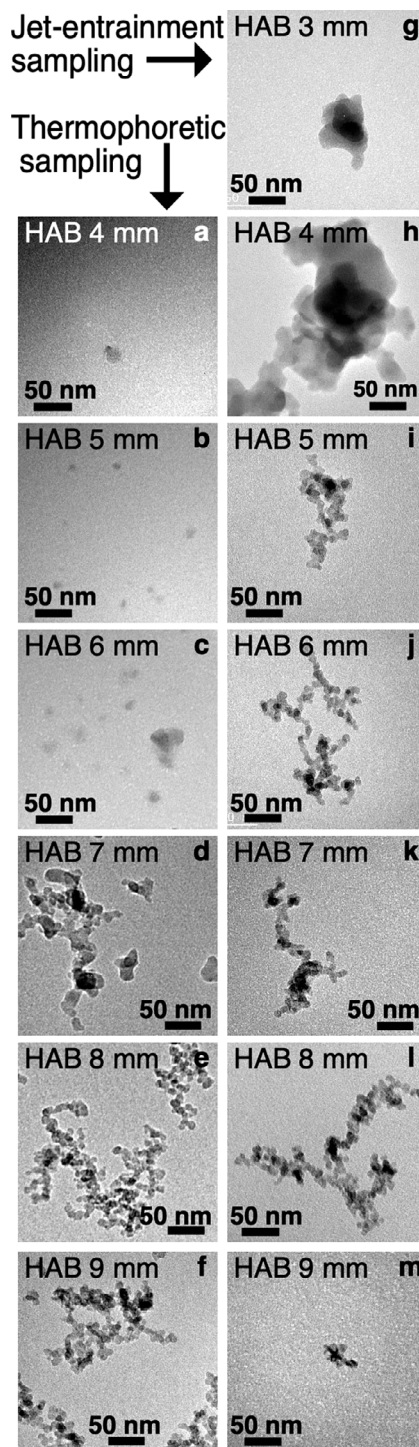


Fig. 2. TEM images of particles extracted from Flame E1. TEM images are shown for particles extracted using (a)–(f) rapid-insertion thermophoretic sampling and (g)–(m) jet-entrainment sampling. The HAB for extraction is given in each panel.

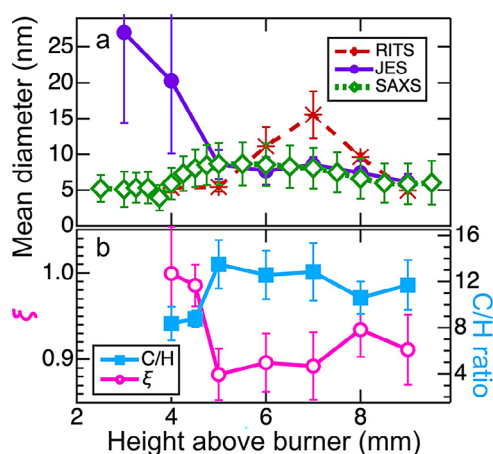


Fig. 3. Primary-particle diameters, dispersion exponent values, and C/H ratios for Flame E1. (a) Mean diameters from TEM images of RITS- and JES-extracted particles are compared with values from SAXS fits using a fractal core-shell model [50]. For JES, we examined ~500 primary particles at each HAB between 5 and 8 mm, 61 at 3 mm, 91 at 4 mm, and 34 at 9 mm [50]. Comparable numbers were examined for RITS. (b) C/H ratios were inferred from the dispersion exponent ξ measured with LII [42, 49].

of magnitude larger than those extracted at 3 mm, the nearly spherical primary particles are smaller and have an average diameter of 20.2 ± 10.1 nm. At HABs of 5 mm (Fig. 2i) and above (Figs. 2j–2m), TEM images of particles extracted with JES show mature soot aggregates of monodisperse primary particles. The average size of the aggregates increases between 5 and 6 mm, is approximately constant between 6 and 8 mm, and then decreases dramatically from 8 to 9 mm. Fig. 3a shows a comparison of average primary particle sizes derived from TEM images of particles extracted using RITS and JES.

Using laser-induced incandescence (LII) to probe Flame E1, Johansson et al. [42] measured the dispersion exponent ξ (Fig. 3b) and demonstrated that soot particles reached full maturity by an HAB of 5 mm. ξ decreases with increasing maturity, and values ≤ 1 indicate mature soot. Atomic C/H ratios, shown in Fig. 3b, were inferred from these measurements using a relationship provided previously [49]. Incipient soot particles have a C/H ratio of 1.4–2.5 [49]. This ratio increases with maturity; mature particles have a ratio of 8–20 [49]. As shown in Fig. 3b, at HABs of 5 mm and higher, the particles are mature. The TEM images shown in Fig. 2 for JES particles are consistent, indicating mature particles by 5 mm, whereas RITS particles appear to be sparse, spherical, translucent monomers, *i.e.*, young particles, at HABs up to 6 mm.

Results using small-angle X-ray scattering (SAXS) to probe Flame E1 (Fig. 3a) are consistent

with the LII results [50]. SAXS measurements are complementary to those of LII. Whereas LII is only sensitive to mature and nearly mature soot particles [51], SAXS is sensitive to incipient and young soot particles as well as mature particles. SAXS measurements demonstrate particle formation at lower HABs than LII.

Fits to SAXS measurements at an HAB of 3 mm in this flame suggest that particles are better represented by a monomer model than by an aggregate model [50]. Fits to the SAXS data using a fractal core-shell model yield a mean monomer diameter of 5.10 ± 2.45 nm and indicate that the particles are internally homogeneous. Internally homogeneous particles are consistent with young soot particles that have not developed the core-shell structure observed for mature soot particles. The results from the SAXS retrievals should be viewed with caution at low HABs, however, because the signal is extremely small and difficult to distinguish from gas-phase signal [52], and the results are model dependent.

At 3 mm, the particles are likely young and not graphitic, hence not observable by LII, and small, as indicated by the SAXS analysis. They appear to coagulate during JES extraction but not into spherical particles; they may be a viscous, gloopy material that leads to partial coalescence during coagulation and larger apparent primary-particle sizes following extraction.

At 4 mm, the SAXS data can be fit using a fractal core-shell model, yielding a primary-particle size of 5.91 ± 2.20 nm with signs of core-shell structure [50]. The suggestion of core-shell structure may indicate that the particles are starting to mature, which is consistent with the observation of LII signal at this HAB [50]. The particles extracted using JES indicate larger aggregates with smaller primary structures than at 3 mm, perhaps suggesting that the primary particles are more viscous at 4 mm than at 3 mm but are still fluid enough to form blobby structures, rather than dendritic aggregates, when coagulated during extraction. The average primary-particle size of the RITS-extracted particles is consistent with the SAXS analysis at 4 mm, as shown in Fig. 3, but the inconsistencies between RITS and other techniques at other HABs makes the RITS results questionable. This result is consistent with previous studies demonstrating significant perturbations to flames by RITS [11,23].

Coagulation of these particles is advantageous for chemical speciation using aerosol mass spectrometry (AMS) because it allows incipient particles to grow to sufficient size (> 50 nm) to be focused into a beam and transmitted to the detection region in an aerodynamic lens (ADL) system [36,37]. In this flame, coagulation of particles sampled at 3 or 4 mm to the sizes shown in Figs. 2g and 2h have allowed AMS data to be collected at these HABs in Flame E1 [42].

At larger HABs, the SAXS measurements are best fit assuming a fractal structure. These results are qualitatively consistent with the TEM images from JES-extracted particles but not with RITS-extracted particles. The SAXS results for primary-particle sizes are also consistent with those inferred from JES-extracted particles between 5 and 9 mm; however, the RITS-extracted particles are only consistent with the SAXS data at 9 mm, as shown in Fig. 3.

3.2. Simulations

Simulations of the steady-state temperature field are shown in Fig. 4 for conditions without and with sampling at an HAB of 6 mm. As shown in Fig. 4c, the jet creates a strong shear layer that strains the flame products between the N_2 flow and entrained gas stream below the probe. Despite the seemingly high shear rate, a separation of hot and cold temperature regions within the sampling probe indicates that mixing remains limited in the laminar flow within the probe. There are large perturbations to the flame at HABs above the jet but relatively small perturbations to the flame below the JES-extraction stream (Fig. 4c), to the side of the jet (Fig. 4d), and to the side, 1 mm from the center of the jet (Fig. 4e). Entrainment of flame gases and particles occurs predominantly at the bottom of the jet, where temperature perturbations are relatively small. This technique thus achieves the goal

of minimizing perturbations to the flame prior to sampling, *i.e.*, on the burner side of the sampling location for co-flow diffusion of premixed flames.

To compare the mixture state after extraction with the centerline mixture state of the unperturbed flame at the same height, we performed Lagrangian analysis of trajectories of different flow variables along the streamline originating at $(x, y, z) = (0, 0, 0)$ for the two flame configurations. For increasing HABs (z), the streamline remains at $x = 0$ and $y = 0$ and is purely vertical for the unperturbed flame and is pushed by the N_2 jet into the probe during sampling. The flow is further accelerated by the N_2 jet during sampling; the evolving mixture state is thus analyzed with respect to the flow residence time $\tau_{res} = \int [1/|U|(s)]ds$ along the streamline with velocity magnitude $|U|(s)$, where s is the streamline abscissa. To examine the mixing between the different streams, we introduced three mixture fractions from the elemental mass fractions Y_C and Y_O of carbon and oxygen atoms: $Z_f = Y_C/Y_C^f$ for the fuel stream, $Z_a = Y_O/Y_O^f$ for the air, and $Z_{N_2} = 1 - Z_a - Z_f$ for the pure N_2 stream.

Fig. 5 shows results of this Lagrangian analysis in terms of temperature and mixture fraction. The jet only marginally affects the flame for $z < 5$ mm when the jet is positioned at $z = 6$ mm, despite rapid thermal quenching from 1800 K to below 700 K within 2 ms with the crossflow jet. The mixing results show that a dilution of almost 60% is achieved after entrainment within the sampling probe. To evaluate how much additional oxygen is entrained within the probe, which can lead to secondary soot oxidation, mixture fractions of air and fuel are also shown as normalized by $(1 - Z_{N_2})$. This normalization enables a comparison with the unperturbed

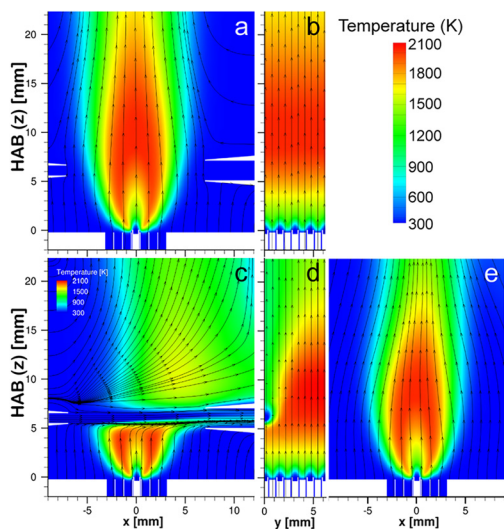


Fig. 4. Simulations of temperature fields and streamlines for the unperturbed and perturbed flame. Contour plots of temperature are shown with streamlines for the unperturbed flame (top) viewed along the (a) y axis (end on, $y = 0$) and (b) x axis (side view, $x = 0$) and for the perturbed flame (bottom) along the (c) y axis (end on, $y = 0$) (d) x axis (side view, $x = 0$), and (e) y axis (end on, $y = 1$ mm).

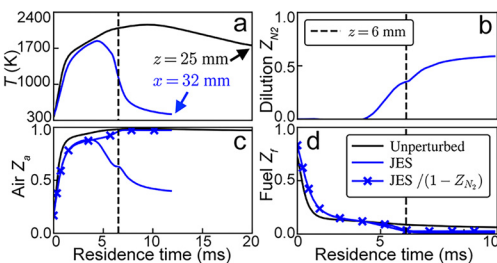


Fig. 5. Time-evolution of temperature and mixture fractions of the three streams along the streamline passing through the origin $(x, y, z) = (0, 0, 0)$ in the unperturbed and JES flow configurations. The dashed vertical lines indicate the residence time at which an HAB (z) of 6 mm is reached in the unperturbed flow vertical centerline streamline. Time histories are shown for (a) temperature, (b) N_2 , (c) flame gas, and (d) fuel mixture fraction. (a) Temperatures are shown for the unperturbed flame along the centerline, ending at an HAB (z) of 25 mm. For the sample that starts at the centerline and is extracted at 6 mm, the final location is 32 mm from the centerline, *i.e.*, 25 mm in the collection probe.

flame for which $Z_{N_2} = 0$ everywhere. The results show that the jet slightly reduces the oxygen-to-fuel ratio compared to the unperturbed flame. These results suggest that JES does not alter the oxidizer composition of the probe sample and that the mixture state extracted is generally representative of the unperturbed flame.

4. Conclusions

We have developed a jet-entrainment sampling (JES) technique for extracting gas-phase species and particles from flames. We have compared TEM results of particles extracted from a co-flow diffusion flame using rapid-insertion thermophoretic sampling (RITS) and the JES technique. At most HABs, results from these sampling techniques are qualitatively very different from one another. RITS-extracted particles are inconsistent with results from *in situ* diagnostics, *i.e.*, LII and SAXS. In contrast, TEM images of JES-extracted particles are consistent with LII and SAXS results and demonstrate good agreement with primary-particle sizes inferred from SAXS measurements at HABs at which the particles are mature aggregates.

At lower HABs, where the particles are less mature, JES appears to lead to coagulation and partial coalescence of highly viscous particles. These results indicate that JES offers benefits over other methods for mature particles but is prone to coagulation of small, young particles. Although a drawback for measurements of particle morphology and size, coagulation poses no problem for particle chemical speciation. In fact, coagulation is a benefit for aerosol mass spectrometry of young particles that would otherwise be too small to pass through an ADL system for detection. Coagulation is much preferred to perturbations to the chemical pathways of precursor species that are introduced by probes inserted into flames, and for these applications, JES is a significant improvement over other methods for speciation of incipient and young soot particles.

Declaration of Competing Interest

The authors declare that they have no known competing financial interests or personal relationships that could have appeared to influence the work reported in this paper.

Acknowledgements

EB and MI were supported by the Office of Science, Office of Basic Energy Sciences (BES), the U.S. Department of Energy (DOE) under award DE-SC0021129. HAM, PES, KOJ, and MFC were funded by the Division of Chemical Sciences,

Geosciences, and Biosciences, BES, DOE. HAM was also supported by this program under a sub-contract to the University of Colorado Boulder from Sandia (FWP 22-022187). RPB was funded by the Sandia Laboratory Directed Research and Development (LDRD) Program. Sandia National Laboratories is a multi-mission laboratory managed and operated by National Technology & Engineering Solutions of Sandia, LLC, a wholly owned subsidiary of Honeywell International Inc. for the DOE's National Nuclear Security Administration under contract DE-NA0003525. The views expressed in the article do not necessarily represent the views of the DOE or the U.S. Government.

References

- [1] R. Strobel, S.E. Pratsinis, Flame aerosol synthesis of smart nanostructured materials, *J. Mater. Chem.* 17 (2007) 4743–4756.
- [2] H. Wang, Formation of nascent soot and other condensed-phase materials in flames, *Proc. Combust. Inst.* 33 (2011) 41–67.
- [3] H.A. Michelsen, Probing soot formation, chemical and physical evolution, and oxidation: a review of *in situ* diagnostic techniques and needs, *Proc. Combust. Inst.* 36 (2017) 717–735.
- [4] P. Desgroux, X. Mercier, K.A. Thomson, Study of the formation of soot and its precursors in flames using optical diagnostics, *Proc. Combust. Inst.* 34 (2013) 1713–1738.
- [5] A.T. Hartlieb, B. Atakan, K. Kohse-Höinghaus, Effects of a sampling quartz nozzle on the flame structure of a fuel-rich low-pressure propene flame, *Combust. Flame* 121 (2000) 610–624.
- [6] P. Desgroux, L. Gasnot, J.F. Pauwels, L.R. Sochet, A comparison of ESR and LIF hydroxyl radical measurements in flame, *Combust. Sci. Technol.* 100 (1994) 379–384.
- [7] J. Biordi, C.P. Lazzara, J.F. Papp, Molecular beam mass spectrometry applied to determining the kinetics of reactions in flames: 1. Empirical characterization of flame perturbation by molecular beam sampling probes, *Combust. Flame* 23 (1974) 73.
- [8] O.I. Smith, D.W. Chandler, An experimental study of probe distortions to the structure of one-dimensional flames, *Combust. Flame* 63 (1986) 19.
- [9] E.L. Knuth, Composition distortion in MBMS sampling, *Combust. Flame* 103 (1995) 171.
- [10] P. Desgroux, L. Gasnot, J.F. Pauwels, L.R. Sochet, Correction of LIF temperature measurements for laser absorption and fluorescence trapping in a flame: application to the thermal perturbation study induced by a sampling probe, *Appl. Phys. B* 61 (1995) 401–407.
- [11] J. Lee, I. Altman, M. Choi, Design of thermophoretic probe for precise particle sampling, *J. Aerosol Sci.* 39 (2008) 418–431.
- [12] U. Struckmeier, P. Obwald, T. Kasper, L. Böhring, M. Heusing, M. Köhler, A. Brockhinke, K. Kohse-Höinghaus, Sampling probe influences on temperature and species concentrations in molecular beam mass spectrometry investigations of flat premixed low-pressure flames, *Z. Phys. Chem. (Munich)* 223 (2009) 503–537.

- [13] F.X. Ouf, J. Yon, P. Ausset, A. Coppalle, M. Maillé, Influence of sampling and storage protocol on fractal morphology of soot studied by transmission electron microscopy, *Aerosol Sci. Technol.* 44 (2010) 1005–1017.
- [14] M. Sirignano, A. D'Anna, Effect of sampling probe perturbation on particle size distribution functions in a slightly sooting premixed flame of ethylene: a modeling study, *Combust. Sci. Technol.* 184 (2012) 1011–1021.
- [15] P.A. Skovorodko, A.G. Tereshchenko, O.P. Korobeinichev, D.A. Knyazkov, A.G. Shmakov, Experiment and numerical study of probe-induced perturbations of the flame structure, *Combust. Theor. Model.* 17 (2013) 1–24.
- [16] L. Deng, A. Kempf, O. Hasemann, O.P. Korobeinichev, I. Wlokas, Investigation of the sampling nozzle effect on laminar flat flames, *Combust. Flame* 162 (2015) 1737–1747.
- [17] C. Saggese, A. Cuoci, A. Frassoldati, S. Ferrarini, J. Camacho, H. Wang, T. Faravelli, Probe effects in soot sampling from a burner-stabilized stagnation flame, *Combust. Flame* 167 (2016) 184–197.
- [18] D. Stepowski, D. Puechberty, M.J. Cottureau, Use of laser-induced fluorescence of OH to study the perturbation of a flame by a probe, *Proc. Combust. Inst.* 18 (1981) 1567–1573.
- [19] A. De Filippo, L.A. Sgro, G. Lanzaolo, A. D'Alessio, Probe measurements and numerical model predictions of evolving size distributions in premixed flames, *Combust. Flame* 156 (2009) 1744–1754.
- [20] N. Hansen, R.S. Tranter, K. Moshhammer, J.B. Randazzo, J.P.A. Lockhart, P.G. Fugazzi, T. Tao, A.L. Kastengren, 2D-imaging of sampling-probe perturbations in laminar premixed flames using Kr X-ray fluorescence, *Combust. Flame* 181 (2017) 214–224.
- [21] N. Hansen, R.S. Tranter, J.B. Randazzo, J.P.A. Lockhart, A.L. Kastengren, Investigation of sampling-probe distorted temperature fields with X-ray fluorescence spectroscopy, *Proc. Combust. Inst.* 37 (2019) 1401–1408.
- [22] J. Lee, S.Y. Yang, A study of stability and vibration for particle sampling probes, *Int. J. Mech. Sci.* 76 (2013) 152–157.
- [23] M.L. Botero, J. Akroyd, D. Chen, M. Kraft, J.R. Agudelo, On the thermophoretic sampling and TEM-based characterisation of soot particles in flames, *Carbon* 171 (2021) 711–722.
- [24] R.A. Dobbins, R.A. Fletcher, W. Lu, Laser microprobe analysis of soot precursor particles and carbonaceous soot, *Combust. Flame* 100 (1995) 301–309.
- [25] R.A. Dobbins, R.A. Fletcher, H.-C. Chang, The evolution of soot precursor particles in a diffusion flame, *Combust. Flame* 115 (1998) 285–298.
- [26] C.M. Megaridis, R.A. Dobbins, Comparison of soot growth and oxidation in smoking and non-smoking ethylene diffusion flames, *Combust. Sci. Technol.* 66 (1989) 1–16.
- [27] Ü.Ö. Köylü, C.S. McEnally, D.E. Rosner, L.D. Pfefferle, Simultaneous measurements of soot volume fraction and particle size/microstructures in flames using a thermophoretic sampling technique, *Combust. Flame* 110 (1997) 494–507.
- [28] R.A. Dobbins, C.M. Megaridis, Morphology of flame-generated soot as determined by thermophoretic sampling, *Langmuir* 3 (1987) 254–259.
- [29] R.A. Dobbins, Hydrocarbon nanoparticles formed in flames and Diesel engines, *Aerosol Sci. Technol.* 41 (2007) 485–496.
- [30] R.L. Vander Wal, Soot precursor material: visualization via simultaneous LIF-LII and characterization via TEM, *Proc. Combust. Inst.* 26 (1996) 2269–2275.
- [31] H. Ghiassi, P. Toth, I.C. Jaramillo, J.S. Lighty, Soot oxidation-induced fragmentation: part 1: the relationship between soot nanostructure and oxidation-induced fragmentation, *Combust. Flame* 163 (2016) 179–187.
- [32] M.M. Maricq, An examination of soot composition in premixed hydrocarbon flames via laser ablation particle mass spectrometry, *J. Aerosol Sci.* 40 (2009) 844–857.
- [33] M.M. Maricq, Size and charge of soot particles in rich premixed ethylene flames, *Combust. Flame* 137 (2004) 340–350.
- [34] E. Goudeli, A.J. Gröhn, S.E. Pratsinis, Sampling and dilution of nanoparticles at high temperature, *Aerosol Sci. Technol.* 50 (2016) 591–604.
- [35] A.D. Abid, J. Camacho, D.A. Sheen, H. Wang, Quantitative measurement of soot particle size distribution in premixed flames - The burner-stabilized stagnation flame approach, *Combust. Flame* 156 (2009) 1862–1870.
- [36] K.O. Johansson, T. Dillstrom, M. Monti, F. El Gabaly, M.F. Campbell, P.E. Schrader, D.M. Popolan-Vaida, N.K. Richards-Henderson, K.R. Wilson, A. Violi, H.A. Michelsen, Formation and emission of large furans and oxygenated hydrocarbons from flames, *Proc. Natl. Acad. Sci. U. S. A.* 113 (2016) 8374–8379.
- [37] K.O. Johansson, J.Y.W. Lai, S.A. Skeen, D.M. Popolan-Vaida, K.R. Wilson, N. Hansen, A. Violi, H.A. Michelsen, Soot precursor formation and limitations of the stabilomer grid, *Proc. Combust. Inst.* 35 (2015) 1819–1826.
- [38] G.D. Ulrich, B.A. Milnes, N.S. Subramanian, Particle growth in flames. II: experimental results for silica particles, *Combust. Sci. Technol.* 14 (1976) 243–249.
- [39] H.H. Grotheer, K. Hoffmann, K. Wolf, S. Kanjarkar, C. Wahl, M. Aigner, Study of carbonaceous nanoparticles in premixed C₂H₄-air flames and behind a spark ignition engine, *Combust. Flame* 156 (2009) 791–800.
- [40] H.H. Grotheer, K. Wolf, K. Hoffmann, Photoionization mass spectrometry for the investigation of combustion generated nascent nanoparticles and their relation to laser induced incandescence, *Appl. Phys. B* 104 (2011) 367–383.
- [41] M.F. Campbell, A. Bohlin, P.E. Schrader, R.P. Bambha, C.J. Klier, B. Johansson, H.A. Michelsen, Design and characterization of a linear Hencken-type burner, *Rev. Sci. Instrum.* 87 (2016) 115114.
- [42] K.O. Johansson, F. El Gabaly, P.E. Schrader, M.F. Campbell, H.A. Michelsen, Evolution of maturity levels of particle surface and bulk during soot growth and oxidation in a flame, *Aerosol Sci. Technol.* 51 (2017) 1333–1344.

- [43] A. Cuoci, A. Frassoldati, T. Faravelli, H. Jin, Y. Wang, K. Zhang, P. Glarborg, F. Qi, Experimental and detailed kinetic modeling study of PAH formation in laminar co-flow methane diffusion flames, *Proc. Combust. Inst.* 34 (2013) 1811–1818.
- [44] A. Cuoci, A. Frassoldati, T. Faravelli, E. Ranzi, Numerical modeling of laminar flames with detailed kinetics based on the operator-splitting method, *Energy Fuels* 27 (2013) 7730–7753.
- [45] W. Pejpichestakul, A. Cuoci, A. Frassoldati, M. Pelucchi, A. Parente, T. Faravelli, Buoyancy effect in sooting laminar premixed ethylene flame, *Combust. Flame* 205 (2019) 135–146.
- [46] W. Pejpichestakul, E. Ranzi, M. Pelucchi, A. Frassoldati, A. Cuoci, A. Parente, T. Faravelli, Examination of a soot model in premixed laminar flames at fuel-rich conditions, *Proc. Combust. Inst.* 37 (2019) 1013–1021.
- [47] H.A. Michelsen, M.B. Colket, P.-E. Bengtsson, A. D’Anna, P. Desgroux, B.S. Haynes, J.H. Miller, G.J. Nathan, H. Pitsch, H. Wang, A review of terminology used to describe soot formation and evolution under combustion and pyrolytic conditions, *ACS Nano* 14 (2020) 12470–12490.
- [48] R.L. Vander Wal, Onset of carbonization: spatial location via simultaneous LIF-LII and characterization via TEM, *Combust. Sci. Technol.* 118 (1996) 343–360.
- [49] H.A. Michelsen, Effects of maturity and temperature on soot density and specific heat, *Proc. Combust. Inst.* 38 (2021) 1197–1205.
- [50] H.A. Michelsen, M.F. Campbell, K.O. Johansson, I.C. Tran, P.E. Schrader, R.P. Bambha, E. Cenker, J.A. Hammons, C. Zhu, E. Schaible, T. Van Buuren, Soot-particle core-shell and fractal structures from small-angle X-ray scattering measurements in a flame, *Carbon N Y* 196 (2022) 440–456.
- [51] H.A. Michelsen, C. Schulz, G.J. Smallwood, S. Will, Laser-induced incandescence: particle diagnostics for combustion, atmospheric, and industrial applications, *Prog. Energy Combust. Sci.* 51 (2015) 2–48.
- [52] H.A. Michelsen, M.F. Campbell, I.C. Tran, K.O. Johansson, P.E. Schrader, R.P. Bambha, J.A. Hammons, E. Schaible, C. Zhu, T. Van Buuren, Distinguishing gas-phase and nanoparticle contributions to small-angle scattering in X-ray scattering reacting aerosol flows, *J. Phys. Chem. A* 126 (2022) 3015–3026.